arXiv:1012.0643v2 [cond-mat.mes-hall] 14 Oct 2011

Electronic topological transition in sliding bilayer graphene

Young-Woo Son,[1,*] Seon-Myeong Choi,[1,2] Yoon Pyo Hong,[1] Sungjong Woo,[1] and Seung-Hoon Jhi[2,3,†]

[1] *Korea Institute for Advanced Study, Seoul 130-722, Korea.*

[2] *Department of Physics, Pohang University of Science and Technology, Pohang 790-784, Korea.*

[3] *Division of Advanced Materials Science, Pohang University of Science and Technology, Pohang 790-784, Korea.*

We demonstrate theoretically that the topology of energy bands and Fermi surface in bilayer graphene undergoes a very sensitive transition when an extremely tiny lateral interlayer shift occurs in arbitrary directions. The phenomenon originates from a generation of an effective non-Abelian vector potential in the Dirac Hamiltonian by the sliding motions. The characteristics of the transition such as pair annihilations of massless Dirac fermions are dictated by the sliding direction owing to a unique interplay between the effective non-Abelian gauge fields and Berry's phases associated with massless electrons. The transition manifests itself in various measurable quantities such as anomalous density of states, minimal conductivity, and distinct Landau level spectrum.

PACS numbers: 73.22.Pr,71.20.-b,81.05.ue,61.48.Gh

I. INTRODUCTION

Changes in the topology of Fermi surfaces known as Lifshitz transition[1] alter physical properties of metals signifcantly[1–3]. Though such an electronic topological transition (ETT) has been pursued in various materials, its realization requires large external perturbations such as alloying or applying high pressure that hinder clear detections of the transition[1–4]. Recent progress in measuring low energy electronic structures of bilayer graphene (BLG)[5–8] provides a new opportunity to explore the ETT because of its unique electronic structures and because of the possible noninvasive control of chemical potential of the system[9].

In BLG, two coupled hexagonal lattices of carbon atoms are arranged according to Bernal stacking[10–15]. Because BLG has a large degeneracy at the charge neutral point[10–15], there have been intense discussions on possible many-body effects in the system[8,9,16–19] Moreover, since electrons in a single layer graphene (SLG) behave as relativistic massless fermions[15], BLG provides a unique playground to control interactions between relativistic particles coupled with the relative mechanical motions of two layers. Hence, the effects of rotational stacking fault on physical properties of BLG have been studied extensively[6,20–22]: however, the effect of sliding one layer with respect to the other has not. This mechanical motion is important because the interactions between the two layers are sensitive to the deviation from Bernal stacking[20–22] and extremely small sliding will change its low energy electronic structures significantly.

In this paper, we predict a very sensitive topological change in the energy bands and Fermi surfaces of BLG when sliding motion or interlayer shear occurs. It is demonstrated that a peculiar coupling between the effective gauge potential with SU(4) symmetry generated by sliding motions and Berry's phase of massless Dirac fermions play a crucial role to change the topology of low energy bands of BLG. It gives rise to either pair annihilations of massless Dirac fermions or generations of fermions by absorbing fermions with topological charges, depending on sliding directions. This will offer new opportunities to realize the ETT driven by non-Abelian gauge fields with gentle maneuverable mechanical operations.

We start with a detailed description of our first-principles calculation methods including a correction for interlayer dispersive forces. The energetics and changes of the interlayer distance for sliding BLG are presented also. Then, the low energy electronic structures obtained by the calculation are discussed when BLG experiences very small sliding between the two layers. The next three sections introduce a model Hamiltonian for the system and discuss the role of gauge potential and Berry's phase for the changes in low energy electronic structures. Several spectroscopic consequences will be discussed in the final section.

II. FIRST-PRINCIPLES CALCULATION METHODS AND ATOMIC STRUCTURES

Our electronic structure calculation employs the first-principles self-consistent pseudopotential method[23] using the generalized gradient approximation (GGA) for exchange-correlation functional emplemented by Perdew, Burke, and Ernzerhof (PBE)[24]. A kinetic energy cutoff for wavefunction of 65 Rydberg is employed and a plane-wave basis set is used. The ion core of carbon atom is described by ultrasoft pseudopotential[25]. A k-point sampling of $60 \times 60 \times 1$ k points uniformly distributed in the two-dimensional Brilouin zone (BZ) is used in self-consistent calculations and $150 \times 150 \times 1$ k points is sampled to obtain electronic energy bands on a rectangular grid of 1.2% of the first BZ size around the K-point. Since we have dealt with sub-Angstrom displacements of atoms, we have tested our calculation as increasing the cutoff to 120 Rydberg (corresponding to a kinetic energy cutoff of 480 Rydberg for charge density and potential) finding no differences in results. The total charge was calculated by using the Marzari-Vanderbilt cold smear-

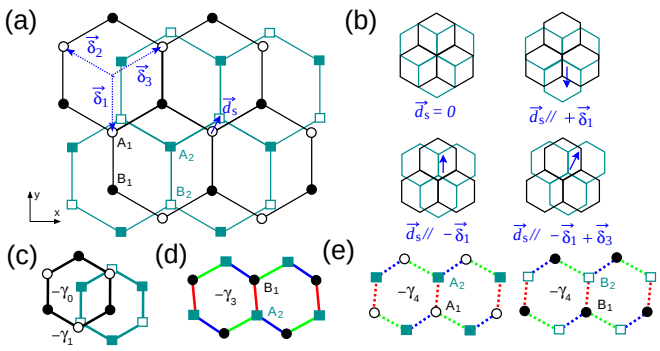

FIG. 1: (color online) (a) In the top (black) and bottom layer (green), two sublattices are denoted by empty (A_1) and filled (B_1) circles and by empty (B_2) and filled (A_2) rectangles, respectively. The bottom layer (layer 2) slides with repect to the top (layer 1) by $\vec{d}_s$. In the top, $\vec{\delta}_1 = (0, -1)a_c$, $\vec{\delta}_2 = (-\frac{\sqrt{3}}{2}, \frac{1}{2})a_c$ and $\vec{\delta}_3 = (\frac{\sqrt{3}}{2}, \frac{1}{2})a_c$. (b) Schematic diagrams for stacking under various sliding directions. (c) The nn intra- and inter-layer hopping parameter, $-\gamma_0$ and $-\gamma_1$. (d) The nnn inter-layer hopping (between B_1-A_2), $-\gamma_3$ with sliding. (e) The smallest inter-layer hopping (between A_1-A_2 or B_1-B_2), $-\gamma_4$ with sliding.

ing scheme[26]. All atomic coordinates are relaxed and the nearest-neighbor carbon-carbon distance (a_c) in a single layer of graphene (SLG) is found to be 1.425 Å. We also perform first-principles calculations again for all different stacking geometries by using another computational package[27] finding no difference.

Since the GGA cannot describe the interlayer interaction between graphene properly, we have employed a seimemprical addition of van der Waals (vdW) forces to our calculations following Grimme's proposal[28]. Within the semiemprical method, the total energy of the system is $E_{\rm PBE+vdW} = E_{\rm PBE} + E_{\rm vdW}$ where $E_{\rm PBE}$ is the total energy from GGA functional of PBE and the total energy given by dispersive forces is $E_{\rm vdW}$ which can be written as $E_{\rm vdW} = -\frac{1}{2}\sum_{i,j} C_{6ij} \sum_{\vec{R}} f_{\rm damp}(|\vec{r}_{ij} + \vec{R}|)|\vec{r}_{ij} + \vec{R}|^{-6}$, where $f_{\rm damp} = s_6 \cdot (1 + e^{-d\cdot(|\vec{r}_{ij}+\vec{R}|/r_0 - 1)})^{-1}$, $\vec{r}_{ij} \equiv \vec{r}_i - \vec{r}_j$ is a vector for carbon-carbon distance, $\vec{R}$ a lattice vector, s_6 a scaling parameter, and d a damping paramter, respectively[28,29]. The coefficient of dispersive forces of C_{6ij} and a sum of vdW radii r_0 are computed for each pair of atoms i and j such that $C_{6ij} = \sqrt{C_{6i}C_{6j}}$ and $r_0 = r_{0i} + r_{0j}$. We have used $C_6 = 1.75$ J nm^6 mol^{-1} and $r_0 = 1.451$ Å for carbon atom suggested by Grimme[28] and $d = 20$, $s_6 = 0.65$ for our GGA calculations. Here, i and j for $E_{\rm vdW}$ run through all atoms in the unit cell and $\vec{R}$ satisfies a criteria of $|\vec{r}_{ij} + \vec{R}| < 100$Å.

Atomic structures of sliding BLG are shown in Figs. 1(a) and 1(b). Without sliding, carbon atoms in BLG are arranged according to Bernal stacking - carbon atoms in one sublattice of the uppler layer are right on top of ones in the other sublattice of the lower layer. When the bottom layer slides with respect to the top layer, the

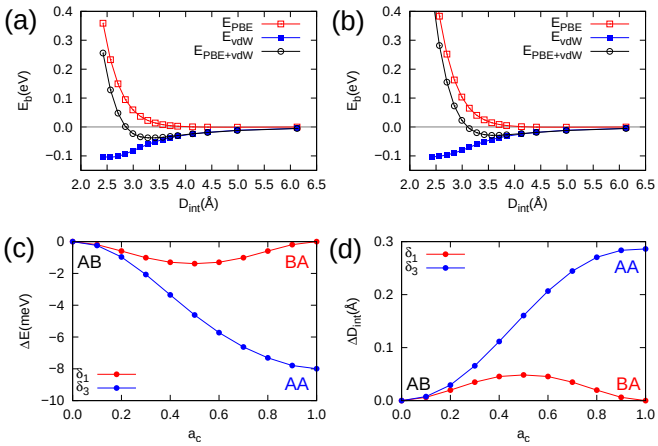

FIG. 2: (color online) Interaction energy per atom (E_b) between two graphene layers (a) with Bernal (AB) stacking and (b) with AA stacking as a function of interlayer distance ($D_{\rm int}$). $E_{\rm PBE}$, $E_{\rm vdW}$ and $E_{\rm PBE+vdW}$ denote the interaction energies calculated by PBE functional only, vdW correction only and including both. Calculations results of $E_{\rm PBE}$ and $E_{\rm PBE+vdW}$ (retangles) are fitted to a second-order Birch equation (solid lines). $E_b = E_{\rm tot} - 2e_{\rm tot}$ where $E_{\rm tot}$ is the total energy of bilayer graphene per atom and $e_{\rm tot}$ that of single layer graphene per atom. In (c) and (d), the variations of binding energy (ΔE) and interlayer distance ($\Delta D_{\rm int}$) with respect to those of AB-stacked bilayer are shown as functions of sliding distance in units of a_c along $\vec{\delta}_1$ (red) and $\vec{\delta}_3$ (blue). The negative ΔE denotes the decrease in binding energy. We set the binding energy and interlayer distance of AB-stacked bilayer to be zero in (a) and (b).

sliding vector $\vec{d}_s$ can be written as a linear combination of $\vec{\delta}_i$ ($i = 1, 2, 3$) which connect the nearest neighbor (nn) carbon atoms in the top layer (For definitions of $\vec{\delta}_i$ ($i = 1, 2, 3$), see Fig. 1). Considering the lattice structures of sliding bilayer, it is easy to check that the sliding along $\pm\vec{\delta}_1$ is equivalent to one along $\pm\vec{\delta}_{2(3)}$. We also note that a sliding along $\vec{\delta}_3$ is equivalent to one along $-\vec{\delta}_1$. Full sliding along $\vec{\delta}_1$ brings an AB-stacking bilayer graphene to a BA-stacking bilayer graphene while one along $\vec{\delta}_3$ shifts an AB-stacking bilayer to a AA-stacking bilayer.

We find that the equilibrium interlayer distance of bilayer graphene (BLG) in Bernal stacking is 3.348Å and its binding energy is 38.76 meV (Fig. 2 (a)), which are in good agreement with other calculations and avaliable experimental data[29–35]. When bilayer graphene has AA-stacking (one layer is right on top of the other layer), the interlayer distance increases to 3.635Å and binding energy decreases to 30.77 meV (Fig. 2 (b)). When one graphene layer slides with respect to the other along either $\vec{\delta}_1$ or $\vec{\delta}_3$ direction, the binding energy starts decreasing and interlayer distance increases agreeing with a previous study[30] (Fig. 2 (c) and (d)). We note that the change in the binding energy (< 0.19 meV) and interlayer distance (<0.01 Å) is quite negligible when the sliding distance is less than 0.14 Å (about 10 % of the

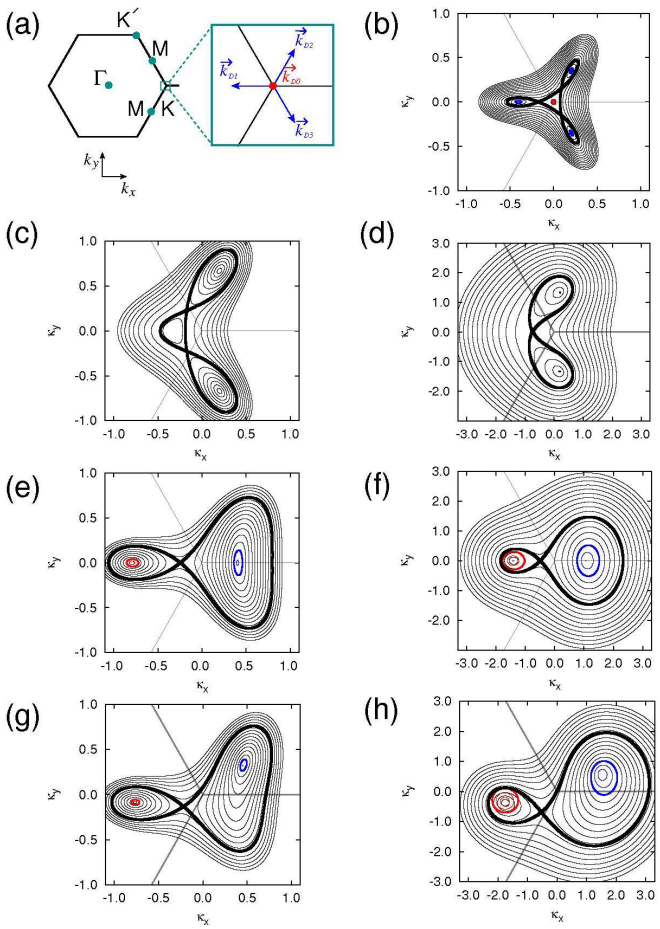

FIG. 3: (a) The small rectangle near around K-point in the first Brillouin zone is enlarged to show the three-fold symmetric vectors $\vec{k}_{D1} = p_D(-1, 0)$, $\vec{k}_{D2} = p_D(1/2, \sqrt{3}/2)$, and $\vec{k}_{D3} = p_D(1/2, -\sqrt{3}/2)$ with respect to $\vec{k}_{D0} = 0$, where $p_D \equiv (2/3a_c)(\gamma_1\gamma_3/\gamma_0^2)$. (b) Energy contour for the valence bands of BLG without sliding. For all panels, $\kappa_x = 100\times(k_x - \overline{\Gamma K})/\overline{\Gamma K}$ and $\kappa_y = 100 \times k_y/\overline{\Gamma K}$. The thick contour is an iso-energy ($E = -1.1$ meV) curve crossing the three saddle points. The blue (red) contours denote the hole (electron) pockets. Energy contours for the valence band of BLG with sliding $\vec{d}_s$ = (c) $0.02\vec{\delta}_1$, (d) $0.1\vec{\delta}_1$, (e) $-0.02\vec{\delta}_1$, (f) $-0.1\vec{\delta}_1$, (g) $0.012(\vec{\delta}_3 - \vec{\delta}_1)$, and (h) $0.1(\vec{\delta}_3 - \vec{\delta}_1)$. The contour interval is set by 0.5 meV for (a), by 1.0 meV for (c), (e) and (g) and by 10 meV for (d), (f) and (h). The thick contours that cross the saddle points are at E = (c) -7.2 meV, (d) -32.7 meV, (e) -10.8 meV, (f) -48.5 meV, (g) -9.7 meV and (h) -74.0 meV.

bond length, a_c).

III. LOW ENERGY BAND STRUCTURES FROM GGA CALCULATIONS

Considering the low energy electronic structure of BLG in Bernal stacking, our calculations show, as in a previous study, four Dirac cones formed around the Fermi energy (E_F) at four Dirac points ($\vec{k}_{Di}$, $i = 0, 1, 2, 3$) near around K-point [Fig. 3(a) and 3(b)][10,11]. The magnitude of $\vec{k}_{Di}$ ($i = 1, 2, 3$) is about 0.4% of the distance between Γ- to K-point ($\overline{\Gamma K}$) [Fig. 3 (b)]. As the energy moves away from the E_F, the four Dirac cones merge to form three saddle points between the cones [Fig. 3(b)]. The calculation result can also be described by an effective Hamiltonian[10],

$$\mathcal{H}_{\rm eff}(\vec{k}) = \hbar v_3 \vec{\tau}\cdot\vec{k} + \frac{\hbar^2 v_0^2}{\gamma_1}(\vec{\tau}^*\cdot\vec{k})\tau_x(\vec{\tau}^*\cdot\vec{k}), \qquad (1)$$

where $v_\alpha = (3/2)\gamma_\alpha a_c/\hbar$ ($\alpha = 0, 3$), $\hbar\vec{k} = \hbar(k_x, k_y)$ is the crystal momentum from K-point, and $\vec{\tau} = (\tau_x, \tau_y)$ and $\vec{\tau}^*$ are Pauli spin matrices and their complex conjugates (See Fig. 1 for definition of γ_α). Typical estimates are $\gamma_0 \simeq 3$ eV, $\gamma_1 \simeq \gamma_3 \simeq \gamma_0/10$ and $\gamma_4 \simeq \gamma_0/20$ (Ref.[36]). We will neglect γ_4 and discuss its role in Sec. VI. If we expand the effective Hamiltonian around each $\vec{k}_{Di}$, we have one isotropic Dirac Hamiltonian, $\mathcal{H}_{D0} = \hbar v_3 \vec{\tau}\cdot\delta\vec{k}_0$ at $\vec{k}_{D0}$, an anisotropic $\mathcal{H}_{D1} = -\hbar v_3(\tau_x^*\delta k_{x1} + 3\tau_y^*\delta k_{y1})$ at $\vec{k}_{D1}$, and two anisotropic others at $\vec{k}_{D2}$ and $\vec{k}_{D3}$ which can be obtained by rotating H_{D1} by $\pm 2\pi/3$ respectively. Here, $\delta\vec{k}_i = (\delta k_{xi}, \delta k_{yi}) = \vec{k} - \vec{k}_{Di}$, ($i = 0, 1, 2, 3$).

We find that the low energy bands of BLG change dramatically when one layer slides with respect to the other in an extremely small amount and in arbitrary directions. Let the bottom layer slide with respect to the top by $\vec{d}_s(= (d_x, d_y))$ [Fig. 1(a) and 1(b)]. First, when the bottom layer moves along $\vec{\delta}_1$ direction by 0.028 Å, i.e., $\vec{d}_s = 0.02\vec{\delta}_1$, only two Dirac cones at $\vec{k}_{D2}$ and $\vec{k}_{D3}$ remain, instead of four cones for BLG without sliding as shown in Fig. 3(c) The energetic position of the saddle points of the valence band decreases from -1.1 meV to -7.2 meV. When the bottom layer slides further ($\vec{d}_s = 0.1\vec{\delta}_1$), the topology changes again and the saddle point energy significantly decreases to -32.7 meV [Fig. 3(d)]. Second, when the bottom layer moves along the direction opposite to the previous one ($\vec{d}_s = -0.02\vec{\delta}_1$), the low energy bands changes again completely. In this case, the Dirac cone at $\vec{k}_{D1}$ moves along the $-k_x$ direction and an anomalous Dirac cone with sickle-shaped energy contours appears at a new Dirac point instead of three cones [Fig. 3(e)]. If the bottom layer slides further by 0.14 Å along $-\vec{\delta}_1$ ($\vec{d}_s = -0.1\vec{\delta}_1$), the topology remains the same and the anomalous cone comes to have an anisotropic shape [Fig. 3(f)]. In this case, the saddle point energy decreases to -48.5 meV (almost 500% of pristine one) [Fig. 3(f)]. Finally, when we slide the bottom layer by $0.012(\vec{\delta}_3 - \vec{\delta}_1)$ [Fig. 3(g)] and $0.1(\vec{\delta}_3 - \vec{\delta}_1)$ [Fig. 3(h)], the topological changes are similar to the case for the sliding along $-\vec{\delta}_1$. The saddle point energy for the sliding by $0.1(\vec{\delta}_3 - \vec{\delta}_1)$ decreases dramatically down to -74.0 meV as shown in Fig. 3(h). After a comprehensive search for the topological changes by the sliding along arbitrary directions (not shown here), we find that the topology of saddle point energy contours is all similar to those shown in Fig. 3(e)-(h)

(one crossing point) except the topologically distinctive phase in Fig. 3(c) (two crossing points).

IV. EFFECTIVE MODEL HAMILTONIANS AND NON-ABELIAN GAUGE POTENTIAL

The hypersensitive topological changes found by first-principles calculations in the previous section demonstrate that the sliding motion creates interactions between the effective non-Abelian SU(4) gauge field background and massless fermions. In the presence of a very tiny sliding, the nnn interlayer interaction (γ_3) is not constant any more but depends exponentially on the different pair distances between carbon atoms in top and bottom layers as shown in Fig. 1(d). The asymmetric inter-layer hopping interaction produces a constant pseudo-gauge potential in the terms of Hamiltonian containing γ_3 only, being similar with an effective Hamiltonian for strained SLG[37–40]. Hence, the effective Hamiltonian for sliding BLG can be written as,

$$\mathcal{H}'_{\rm eff}(\vec{k}) = \hbar v_3 \vec{\tau}\cdot(\vec{k}-\vec{\lambda}) + \frac{\hbar v_3}{p_D}(\vec{\tau}^*\cdot\vec{k})\tau_x(\vec{\tau}^*\cdot\vec{k}) \qquad (2)$$

where $p_D \equiv \gamma_1' v_3/(\hbar v_0^2)$ and γ_1' is the reduced nn interlayer interaction. (See Appendix for derivation of Eq. (2)). We find that the constant vector potential ($\vec{\lambda}$) explicitly depends on the sliding vector, $\vec{\lambda} \equiv (\lambda_x, \lambda_y) = \beta(d_y, -d_x)$. By fitting the energy bands obtained by the model to ones by the first-principles calculation, we can estimate that β is about $1/a_c^2$. The gauge symmetry in Eq. (2) apparently seems to be broken since $\vec{\lambda}$ is absent in the quadratic term of $\vec{k}$. However, when we expand Eq. (1) at each Dirac point ($\vec{k}_{Di}$), the four Dirac cones shift depending on both $\vec{\lambda}$ and their own positions as $\vec{k}_{Di} \to \vec{k}_{Di} + \vec{A}_i(\vec{\lambda})$ ($i = 0, 1, 2, 3$). If $|\vec{\lambda}| \ll p_D$, $\vec{A}_0 = (\lambda_x, \lambda_y)$, $\vec{A}_1 = (-\lambda_x, \frac{\lambda_y}{3})$, $\vec{A}_2 = (-\frac{\sqrt{3}\lambda_y}{3}, -\frac{\sqrt{3}\lambda_x}{3} - \frac{2\lambda_y}{3})$ and $\vec{A}_3 = (\frac{\sqrt{3}\lambda_y}{3}, \frac{\sqrt{3}\lambda_x}{3} - \frac{2\lambda_y}{3})$. So, each Dirac cone moves along a different direction depending on its position.

The essential feature of the system that enables the electronic topological transition in BLG is the shift of four Dirac points along different directions under the sliding of one layer against the other. As we have shown, the effect of sliding is to replace $\delta\vec{k}_i = \vec{k} - \vec{k}_{Di}$ with $\delta\vec{k}_i - \vec{A}_i$ in the effective Hamiltonian for the low energy modes near the Dirac points and this feature suggests that the sliding in BLG induces a non-Abelian background gauge field associted with these modes. In order to show this more explicitly, we assume that before sliding, there are four massless Dirac fermions, labeled by $i = 0, 1, 2, 3$, whose Hamiltonians are all isotropic and of same chirality:

$$\mathcal{H}_{Di} = \hbar v_3 \vec{\tau}^*\cdot\delta\vec{k}_i\,, \quad i = 0, \ldots, 3. \qquad (3)$$

We can then form a quadruplet out of four fermions, so that the index i is now viewed as the "color" index of SU(4) symmetry, and combine the four Hamiltonians $\mathcal{H}_{Di}$ compactly as $\mathcal{H}_D = \hbar v_3(\vec{\tau}^*\cdot\delta\vec{k}) \otimes \mathbf{I}$, where $\mathbf{I}$ is the 4×4 identity matrix. If we now introduce the background gauge field $\vec{\mathbf{A}} = (\mathbf{A}_x, \mathbf{A}_y)$ for the SU(4) symmetry with

$$\mathbf{A}_x = \lambda_x \begin{pmatrix} 1 & & & \\ & -1 & & \\ & & 0 & \\ & & & 0 \end{pmatrix} - \frac{\lambda_y}{\sqrt{3}} \begin{pmatrix} 0 & & & \\ & 0 & & \\ & & 1 & \\ & & & -1 \end{pmatrix},$$

and

$$\mathbf{A}_y = \frac{\lambda_x}{\sqrt{3}} \begin{pmatrix} 0 & & & \\ & 0 & & \\ & & -1 & \\ & & & 1 \end{pmatrix} + \lambda_y \begin{pmatrix} 1 & & & \\ & \frac{1}{3} & & \\ & & -\frac{2}{3} & \\ & & & -\frac{2}{3} \end{pmatrix},$$

so that $\delta\vec{k}\mathbf{I} \to \delta\vec{k}\mathbf{I} - \vec{\mathbf{A}}$ in the Hamiltonian, then Eq. (3) now becomes

$$\mathcal{H}_{Di} = \hbar v_3 \vec{\tau}^*\cdot(\delta\vec{k}_i - \vec{A}_i)\,, \quad i = 0, \ldots, 3, \qquad (4)$$

where $\vec{A}_i$ are precisely the shifts of the Dirac points shown at the beginning of this section. Since both $\mathbf{A}_x$ and $\mathbf{A}_y$ are linear combinations of the generators of SU(4), we now see the effect of sliding as if introducing a non-Abelian background gauge field.

The low energy Hamiltonian of bilayer graphene is different from what we have just shown above in that $\mathcal{H}_{D0}$ has opposite chirality from $\mathcal{H}_{Di}$ for $i = 1, 2, 3$, and that the latter three Hamiltonians are anisotropic. A parity inversion $\delta k_y \to -\delta k_y$ for $\mathcal{H}_{D0}$ and anisotropic rescalings of $\delta\vec{k}_i$ for $\mathcal{H}_{Di}$ ($i = 1, 2, 3$) transform SU(4) isotropic quadruplet to the low energy Hamiltonian of BLG. This transformation is equivalent to multiplying the Pauli matrices τ_x and τ_y with (different) constants in Eq. (4) — for example, $(\tau_x, \tau_y) \to (\tau_x, -\tau_y)$ for $i = 0$, and $(\tau_x, \tau_y) \to -(\tau_x, 3\tau_y)$ for $i = 1$ — thereby breaking the SU(4) symmetry of the previous paragraph. But the structure of the Hamiltonians otherwise remains the same, and in particular, the shifts of the Dirac points are still given by $\vec{A}_i$ of Eq. (4).

V. ROLES OF BERRY'S PHASE IN ELECTRONIC TOPOLOGICAL TRANSITION

The characteristics of the ETT are ruled by unique interplay between the effective non-Abelian vector potential and conservation of Berry's phase. The Berry's phase (ϕ_B) for each Dirac cone at $\vec{k}_{Di}$ can be calculated by using $\phi_B = \oint_\Gamma d\vec{k}\cdot\mathcal{A}(\vec{k})$ where $\mathcal{A}(\vec{k}) = i\langle u_{Di}(\vec{k})|\partial_{\vec{k}}|u_{Di}(\vec{k})\rangle$, Γ is a path enclosing each Dirac point, and $u_{Di}(\vec{k})$ is a single-valued spinor-like eigenfunction of each Dirac Hamiltonian at $\vec{k}_{Di}$. Without sliding, we have $\phi_B = +\pi$ for the massless Dirac fermions around $\vec{k}_{Di}$ ($i = 1, 2, 3$) and $\phi_B = -\pi$ for the ones at the center $\vec{k}_{D0}$ [Fig. 4(a)]. For a path enclosing all Dirac points at higher energy, we

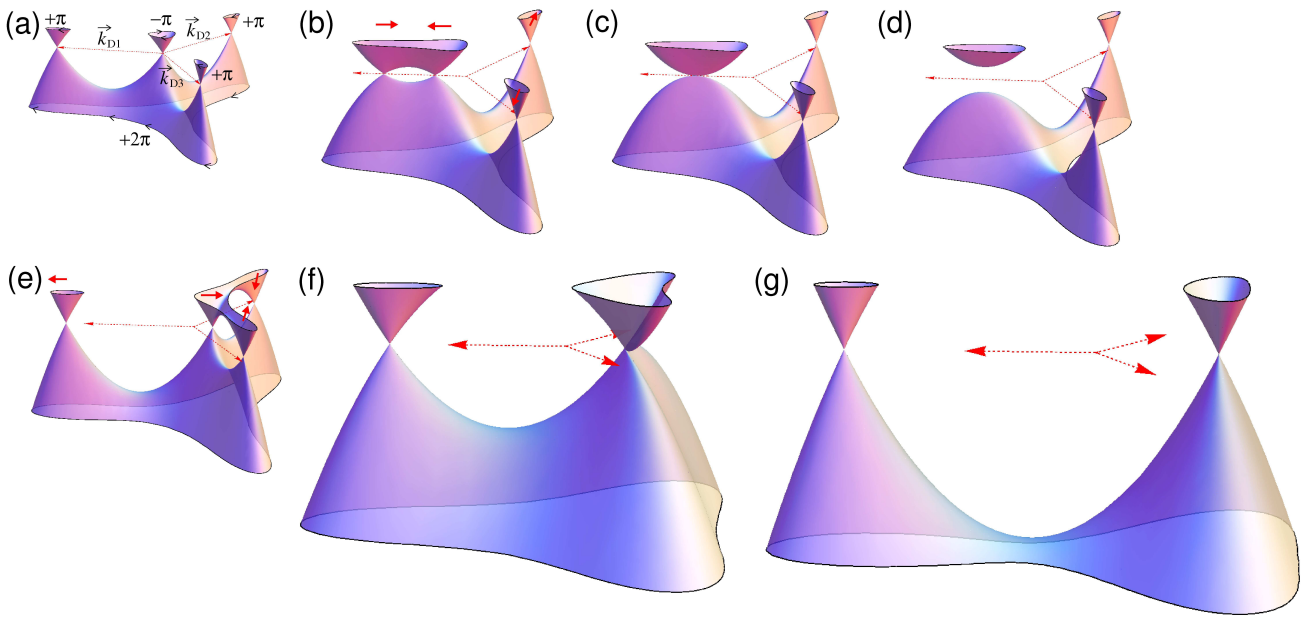

FIG. 4: Three dimensional plots of low energy bands from the effective Hamiltonian of Eq. (1) with $\vec{\lambda} = (\lambda_x, 0)$. (a) Without sliding ($\vec{\lambda} = 0$), three anisotropic Dirac cones with Berry phase π at $\vec{k}_{Di}$ ($i = 1, 2, 3$) denoted by dotted red arrows in all panels, and isotropic one with $-\pi$ at $\vec{k}_{D0}$. Energy bands for sliding BLG with (b) $\lambda_x = -p_D/5$ (c) $-p_D/4$, (d) $-p_D/3$, (e) $p_D/5$, (f) $3p_D/4$ and (g) $1.8p_D$. In term of sliding distance d_y, (b) $d_y \simeq -0.003$, (c) -0.004, (d) -0.005, (e) $+0.003$, (f) $+0.012$ and (g) $+0.029$ Å. The solid red arrows in (b) and (e) indicate the movements of Dirac cones at sliding.

can use the quadratic Hamiltonian (1) and ϕ_B is $+2\pi$[5,9]. So, the total ϕ_B is always conserved to be 2π [Fig. 4(a)][9].

Now, to reveal the role of Berry's phase explicitly, let us consider exactly solvable cases without the assumption of $|\vec{\lambda}| \ll p_D$. For sliding along $\pm\vec{\delta}_1$ direction, i.e., $\vec{d}_s = (0, \mp d_y)$ ($d_y > 0$), the effective vector potential is given by $\vec{\lambda} = (\lambda_x, 0) = (\mp\beta d_y, 0)$. Here, $\lambda_x < 0$ ($\lambda_x > 0$) when sliding along $+\vec{\delta}_1(-\vec{\delta}_1)$ direction. Then we have four different local vector potentials $\vec{A}_i$ for each $\vec{k}_{Di}$ such that

$$\begin{aligned}
\vec{A}_0 &= \frac{p_D}{2}\left(-1 + \sqrt{1 + \frac{4\lambda_x}{p_D}}, 0\right), \\
\vec{A}_1 &= \frac{p_D}{2}\left(+1 - \sqrt{1 + \frac{4\lambda_x}{p_D}}, 0\right), \\
\vec{A}_2 &= \frac{\sqrt{3}p_D}{2}\left(0, -1 + \sqrt{1 - \frac{4\lambda_x}{3p_D}}\right), \\
\vec{A}_3 &= \frac{\sqrt{3}p_D}{2}\left(0, +1 - \sqrt{1 - \frac{4\lambda_x}{3p_D}}\right).
\end{aligned}$$

We note that $\vec{A}_0 + \vec{A}_1 = 0$ and $\vec{A}_2 + \vec{A}_3 = 0$. Thus, the Dirac cone at $\vec{k}_{D0}$ and the one at $\vec{k}_{D1}$ move in opposite direction when bilayer graphene slides along $\pm\vec{\delta}_1$ and so do those at $\vec{k}_{D2}$ and $\vec{k}_{D3}$. It is also noticeable that $\vec{k}_{D0} + \vec{A}_0 = \vec{k}_{D1} + \vec{A}_1$ when $\lambda_x = -p_D/4$ and $\vec{k}_{D1} + \vec{A}_1 = \vec{k}_{D2} + \vec{A}_2 = \vec{k}_{D3} + \vec{A}_3$ when $\lambda_x = 3p_D/4$. Hence, when the bottom layer slides along $-y$ direction ($\vec{\delta}_1$ direction) by $d_y = p_D/(4\beta)$, the two Dirac cones at $\vec{k}_{D0}$ and $\vec{k}_{D1}$ meet at $(-p_D/2, 0)$ while three cones at $\vec{k}_{D1}$, $\vec{k}_{D2}$ and $\vec{k}_{D3}$ meet together at $(p_D/2, 0)$ when sliding along $+y$ direction ($-\vec{\delta}_1$ direction) by $d_y = 3p_D/(4\beta)$.

For the sliding along $+\vec{\delta}_1$ direction, the effective Hamiltonian shown in Eq. (2) can be expanded around $\vec{k}_+ = (-p_D/2, 0)$ so that the resulting Hamiltonian can be written as

$$\mathcal{H}_+ \simeq \hbar v_3 \tau_x \left[\frac{(\delta k_x)^2}{p_D} - \left(\lambda_x + \frac{p_D}{4}\right)\right] + 2\hbar v_3 \tau_y \delta k_y \quad (5)$$

where $\delta\vec{k} = (\delta k_x, \delta k_y) \equiv \vec{k} - \vec{k}_+$ and $\lambda_x < 0$. The new effective Hamiltonian (5) has eigenvalues given by

$$E_+(\delta\vec{k}) = \pm\hbar v_3 \sqrt{\left[\frac{(\delta k_x)^2}{p_D} - \left(\lambda_x + \frac{p_D}{4}\right)\right]^2 + 4(\delta k_y)^2}. \quad (6)$$

So, when $-p_D/4 < \lambda_x < 0$ or $0 < d_y < p_D/(4\beta)$, there are still two Dirac cones at $\vec{k}_{D0} + \vec{A}_0$ and $\vec{k}_{D1} + \vec{A}_1$. When λ_x reaches to a critical value of $-p_D/4$, the Hamiltonian is given by $\hbar v_3 \tau_x (\delta k_x)^2/p_D + 2\hbar v_3 \tau_y \delta k_y$ so that the dispersion along k_x direction is massive while one along k_y direction is still massless. Two other cones at $\vec{k}_{D2} + \vec{A}_2$ and $\vec{k}_{D3} + \vec{A}_3$ move away from each other in $\pm k_y$ direction maintaining their anisotropic Dirac cone shapes. Therefore, it can be seen that the cones at $\vec{k}_{D0}$ and $\vec{k}_{D1}$ merge together when $\vec{\lambda} = (-p_D/4, 0)$ [Fig. 4(c)]. The

corresponding sliding distance of d_y is about 0.3% of a_c ($d_y = p_D/(4\beta) \sim 0.004$Å). The low energy bands already change their topology from the original structure under extremely small sliding. For further sliding, $\lambda_x < -p_D/4$ ($d_y > p_D/(4\beta)$), the merged cone eventually disappears and the spectrum of Eq. (6) develops an energy gap at $\vec{k}_+$ as shown in Fig. 4(d). The gap is linear with sliding distance as given by $2\hbar v_3|\lambda_x + p_D/4| \simeq 2\hbar v_3 \beta d_y \sim 0.9 \times [d_y/a_c]$ eV. The opening of energy gap signals *a pair annihilation of two massless Dirac electrons* with the opposite 'topological charges' of ± 1 since the two Dirac cones at $\vec{k}_{D0}$ and $\vec{k}_{D1}$ have the Berry's phase of $\pm\pi$ respectively. This also confirms the Berry's phase conservation since the remaining two anisotropic Dirac cones at $\vec{k}_{D2}$ and $\vec{k}_{D3}$ give the total ϕ_B of 2π.

Next, for the sliding along $-\vec{\delta}_1$ direction, the effective Hamiltonian can be obtained by expanding Eq. (2) around $\vec{k}_- = (p_D/2, 0)$:

$$\mathcal{H}_- \simeq \hbar v_3 \tau_x^* \left[2\delta k_x + \frac{(\delta k_x)^2 - (\delta k_y)^2}{p_D} + \left(\frac{3p_D}{4} - \lambda_x \right) \right] + 2\hbar v_3 \tau_y^* \frac{(\delta k_x)(\delta k_y)}{p_D}, \quad (7)$$

where $\delta\vec{k} = (\delta k_x, \delta k_y) \equiv \vec{k} - \vec{k}_-$ and $\lambda_x > 0$. When $0 < \lambda_x < 3p_D/4$, there are three Dirac cones at $\vec{k}_{Di} + \vec{A}_i$ ($i = 0, 2, 3$). However, when $\lambda_x = 3p_D/4$, the three Dirac cones merge at $\vec{k}_-$ and this Hamiltonian gives an anomalous dispersion relation written by $E_-(\delta\vec{k}) = \pm\hbar v_3 \sqrt{f^2(\delta\vec{k}) + g^2(\delta\vec{k})}$ where $f(\delta\vec{k}) = 2\delta k_x + (\delta k_x)^2/p_D - (\delta k_y)^2/p_D$ and $g(\delta\vec{k}) = 2(\delta k_x)(\delta k_y)/p_D$. This gives sickle-shaped constant energy contours which are consistent with our *ab initio* calculation results shown in Figs. 3(e) and (g). When $\lambda_x > 3p_D/4$, the effective Hamiltonian (7) does not develop any energy gap at all. Instead, when $\lambda_x \gg 3p_D/4$, the effective Hamiltonian has a Dirac point at $\vec{k}'_- = (-p_D/2 + \sqrt{\lambda_x p_D}, 0)$ and is given by

$$\mathcal{H}'_- \simeq 2\hbar v_3 \sqrt{\frac{\lambda_x}{p_D}} \tau_x^* \delta k_x + 2\hbar v_3 \left(\sqrt{\frac{\lambda_x}{p_D}} - 1 \right) \tau_y^* \delta k_y, \quad (8)$$

where $\delta\vec{k} = (\delta k_x, \delta k_y) \equiv \vec{k} - \vec{k}'_-$. So, as sliding distance increases along $-\vec{\delta}_1$, the anomalous Hamiltonian (7) gradually transforms to the anisotropic Dirac Hamiltonian (8). This is quite contrary to the gapped spectrum (6) generated by sliding motion along $\vec{\delta}_1$ direction ($\mathcal{H}_+$ in Eq. (5)). The other cone at $\vec{k}_{D1} + \vec{A}_1$ moves in $-k_x$ direction maintaining its anisotropic dispersion relation. As $\lambda_x \gg 3p_D/4$, the Dirac cone at $\vec{k}_{D1} + \vec{A}_1$ has an asymtotic shape as following,

$$\mathcal{H}''_- \simeq -2\hbar v_3 \sqrt{\frac{\lambda_x}{p_D}} \tau_x^* \delta k_x - 2\hbar v_3 \left(\sqrt{\frac{\lambda_x}{p_D}} + 1 \right) \tau_y^* \delta k_y, \quad (9)$$

where $\delta\vec{k} = (\delta k_x, \delta k_y) \equiv \vec{k} - \vec{k}_{D1} - \vec{A}_1$. Therefore, in contrast to the first case, no energy gap develops even when the sliding distance is increased further. Instead, the anomalous dispersion transforms to an anisotropic Dirac cone [Fig. 4(g)]. This phenomenon can be interpreted as a merging of two massless fermions of topological charge $+1$ with one of topological charge -1. As a result, *a new fermion of topological charge* $+1$ *is generated*. We note that the total ϕ_B of 2π is conserved since the new particle has ϕ_B of π. Hence, the topological charges of fermionic particles in BLG are strictly governed by Berry's phase conservation rule.

VI. EFFECT OF SMALLEST INTERLAYER HOPPINGS

When sliding occurs, the smallest interlayer interaction γ_4 shown in Fig. 1(e) becomes anisotropic and depends on the pair distances between relevant carbon atoms in the top and bottom layer. This effect adds an additional Hamiltonian to Eq. (2),

$$\mathcal{H}'_{\text{eff}} \simeq \frac{2\hbar^2 v_0 v_4}{\gamma_1} \vec{k} \cdot (\vec{k} + \vec{\lambda}) \tau_0 + \frac{\hbar^2 v_4^2}{\gamma_1} [\vec{\tau}^* \cdot (\vec{k} + \vec{\lambda})] \tau_x [\vec{\tau}^* \cdot (\vec{k} + \vec{\lambda})], \quad (10)$$

where $v_4 = \frac{3\gamma_4 a_c}{2\hbar}$ (See Appendix for derivation of Eq. (10)). Since the second term in Eq. (10) is twenty times smaller than the first term, we will neglect the second term hereafter. When sliding along $\pm\vec{\delta}_1$, the difference between Dirac energies at $\vec{k}_{D1}$ and $\vec{k}_{D0}$ is given by $\frac{2\gamma_1 v_3^2 v_4}{v_0^3}(1 - \frac{\lambda_x}{p_D})\sqrt{1 + \frac{4\lambda_x}{p_D}}$. Without sliding ($\lambda_x = 0$), the difference becomes $\Delta\varepsilon_{\text{eh}} = \frac{2\gamma_1 v_3^2 v_4}{v_0^3}$, which indicates the hole and electron doped Dirac cone at $\vec{k}_{D1}$ and $\vec{k}_{D0}$ respectively. This explains the hole and electron doped cones shown in our *ab initio* calculation results [Fig. 3(b)]. With sliding along $\vec{\delta}_1$, the difference disappears when $\lambda_x < -p_D/4$ as shown in Figs. 3(c) and 3(d) so that all Dirac cones are charge-neutral. Contrary to this, when sliding along $-\vec{\delta}_1$, the difference changes its sign when $\lambda_x > p_D$ and decreases significantly as sliding distance increases. So, the hole-doped Dirac cone at $\vec{k}_{D1}$ changes to be electron-doped and the new Dirac cone to be hole-doped with increasing amount of doping as increasing sliding distance as shown in our first-principles calculations [Figs. 3 (e)-(h)]. We note that variations in γ_4 do not affect any topological changes discussed so far.

VII. DISCUSSION

The direct signatures of the ETT can be readily measured using various experiment methods. We showed that the tiny sliding lifts the degeneracy at E_F as the

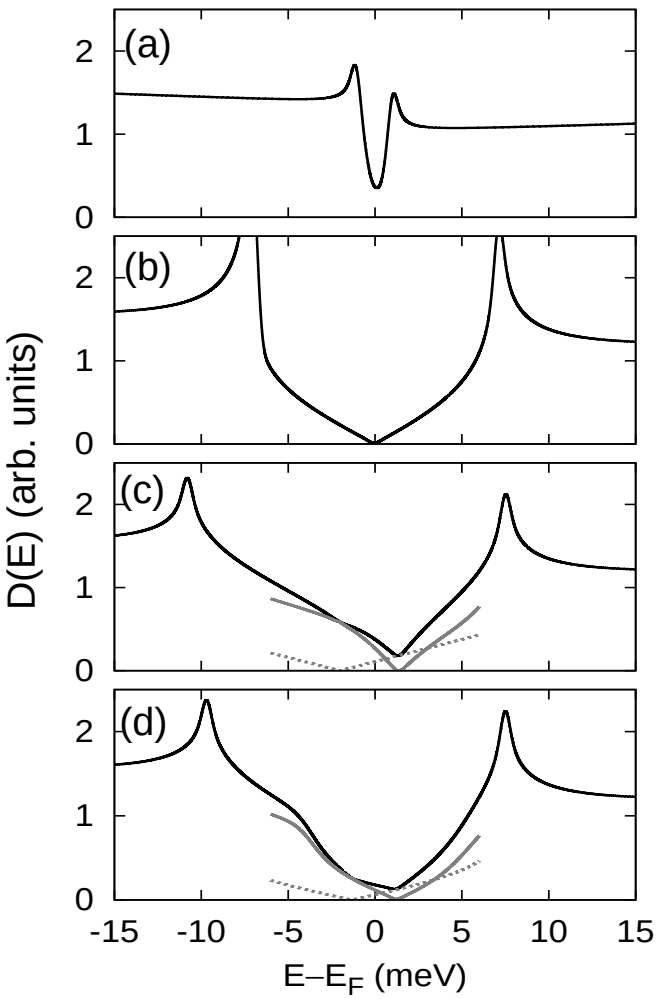

FIG. 5: First-principles calculations of total density of states of sliding BLG when $\vec{d_s}$ = (a) 0, (b) $0.02\vec{\delta}_1$, (c) $-0.02\vec{\delta}_1$, and (d) $0.012(\vec{\delta}_3 - \vec{\delta}_1)$, respectively. The grey solid and dotted lines in (c) and (d) are the partial density of states projected onto $\kappa_x > \kappa_s$ and $\kappa_x < \kappa_s$ region of the BZ in Fig. 3(e) and 3(g), respectively, where κ_s is a x-component of the saddle point of each energy contour.

number of Dirac cones is always reduced from four to two with significant increase of the saddle point energies and deformations of remaining Dirac cones. Therefore, first, high-resolution scanning tunneling microscopy[6,41] can directly measure the changes in the density of states ($D(E)$). Between saddle point energies $|E| < \varepsilon_s$ where $\varepsilon_s = \gamma_1 v_3^2/(4v_0^2)$ without sliding, the total density of states per unit area is given by $D(E) = |E|/(\pi v_3^2)$. When BLG slides along $\pm\vec{\delta}_1$, saddle point energies increase linearly as sliding distance increases, $\varepsilon_s(d_y) = \hbar v_3|\lambda_x - p_D/4| \sim \hbar v_3 \beta d_y$. When sliding along $\vec{\delta}_1$, the two Dirac cones disappear quickly and the other two remaining ones are anisotropic massless Dirac cones. So, the density of states in between saddle point energies $\pm\varepsilon_s(d_y)$ linearly depends on energy, $D(E) \sim |E|$. Our first-principles calculations indeed show drastic variations in the position of van Hove singularity (vHS) below and above the charge neutral point upon sliding (Fig. 5). In between the two vHSs, a linear [Figs. 5(a) and 5(b)] or a mostly square-root dependence of $D(E)$ [Figs. 5(c) and (d)] appears as the sliding direction is changed, which is a unique feature of two-dimensional materials[42,43].

Second, the Landau level (LL) spectrum for a small perpendicular magnetic field (B) also exhibits distinctive dependence on the sliding direction. By using semiclassical quantization rule under the perpendicular magnetic fields (B), $S(E) = \frac{2\pi|e|B}{\hbar c}(n+\gamma)$ and $\partial_E S(E) = 4\pi^2 D(E)$ where $S(E)$ is an area of closed orbit of electron and $\gamma = 1/2 - \phi_B/2\pi$[42,44,45], we can immediately confirm that the Landau level (LL) spectrum under a small magnetic field is given by $E_n \sim \pm(Bn)^{1/2}$ in the case of sliding BLG along $\vec{d_s} = 0.02\vec{\delta}_1$. When BLG slides by either $-0.02\vec{\delta}_1$ or $0.012(\vec{\delta}_3 - \vec{\delta}_1)$, the anomalous Dirac cone shape results in $D(E) \sim \sqrt{E}$ being similar to the previous study on the density of states of semi-Dirac cone (massive in one direction and massless in the other)[42,45]. By using the rule above and $D(E) \sim \sqrt{E}$, the LL spectrum is given by $E_n \sim \pm(Bn)^{2/3}$. It is noticeable that, irrespective of sliding direction, the zeroth LL exists at zero energy since the topological charge conservation (Berry's phase conservation) enforce the existence of at least one massless modes in the system.

Third, an ideal minimal conductivity of $24e^2/(\pi^2\hbar)$ at the charge neutral point[11–13] will decrease quickly when sliding occurs (e is the electron charge). The conductivity of anisotropic massless Dirac fermions with a dispersion, $v_x\tau_x k_x + v_y\tau_y k_y$ is given by $\sigma = g\frac{e^2}{\pi^2\hbar}\frac{v_x}{v_y}$[12] where g is a degeneracy factor ($g = 4$ if considering valley and spin degeneracies) and e is an electron charge. So, by using Eqs (8) and (9), the conductivity in wide BLG sliding along $-\vec{\delta}_1$ ($d_y \gg p_D$) can be calculated easily, $\sigma = \frac{8e^2}{\pi^2\hbar}(1 - p_D/\lambda_x)^{-1} \simeq \frac{8e^2}{\pi^2\hbar}(1 + p_D/\lambda_x)$. The conductivity approaches $8e^2/(\pi^2\hbar)$ as sliding distance increases.

In summary, we show that the topology of energy bands of BLG changes significantly if sliding of extremely small distance occurs in any direction. The effective non-Abelian background gauge potential can be generated by sliding motion and is shown to play an important role in dictating the characteristics of sliding induced ETT. Hence, the ETT driven by non-Abelian gauge fields that are thought to be possible in cold atomic gas[42,43,46] or similar effects in high energy physics[47] can be realizable in sliding BLG.

Note added in proof After submission, we became aware of related works on similar systems from other groups[48–50]

Acknowledgements

Y.-W.S. acknowledges discussions with K. Lee, P. Yi, and K. Novoselov. Y.-W.S. was supported by the NRF grant funded by the Korea government (MEST)

(QMMRC, No. R11-2008-053-01002-0 and Nano R&D program 2008-03670). S.-M.C. and S.-H.J. were supported by NRF funded by MEST (Grant 2009-0087731 and WCU program No. R31-2008-000-10059-0). We thank KIAS for providing computing resources (KIAS CAC Linux Cluster System).

Appendix: Derivation of Eqs. (2) and (10)

A single particle Hamiltonian of BLG in Bernal stacking, $H = H_0 + H_1 + H_2$, can be written as

$$H_0 = -\gamma_0 \sum_{\vec{r},j,\alpha} a^\dagger_\alpha(\vec{r}) b_\alpha(\vec{r}+\vec{\delta}_j) + (\text{h.c.}), \quad (A.1)$$

$$H_1 = -\gamma_1 \sum_{\vec{r}} a^\dagger_1(\vec{r}) b_2(\vec{r}) - \gamma_3 \sum_{\vec{r},j} a^\dagger_2(\vec{r}+\vec{\delta}_j) b_1(\vec{r}) + (\text{h.c.}), \quad (A.2)$$

$$H_2 = -\gamma_4 \sum_{\vec{r},j} a^\dagger_1(\vec{r}+\vec{\delta}_j) a_2(\vec{r}) - \gamma_4 \sum_{\vec{r},j} b^\dagger_1(\vec{r}+\vec{\delta}_j) b_2(\vec{r}) + (\text{h.c.}), \quad (A.3)$$

where H_0 is a Hamiltonian for intra-layer interactions in each SLG and H_1 and H_2 are for inter-layer interactions between two SLG. Here $a^\dagger_\alpha(a_\alpha)$ and $b^\dagger_\alpha(b_\alpha)$ are the creation (annihilaton) operator of π-electron located at A- and B-sublattice of layer α $(= 1, 2)$ respectively, $\vec{r} = m\vec{a}_1 + n\vec{a}_2$ (m and n are integers), $\vec{a}_1 (= \vec{\delta}_3 - \vec{\delta}_1)$ and $\vec{a}_2 (= \vec{\delta}_2 - \vec{\delta}_1)$ are unit vectors of hexagonal lattice of SLG[5,10–12,15]. γ_0 is the intra-layer nn hopping parameter, and γ_1 and γ_3 are for the nn and next nn (nnn) inter-layer hoppings parameters, respectively[5,10–12,15].

Using Fourier transformations of $a_\alpha(\vec{r}) = \frac{1}{\sqrt{N}} \sum_{\vec{p}} e^{-i\vec{p}\cdot\vec{r}} a_{\alpha\vec{p}}$ and $b_\alpha(\vec{r}) = \frac{1}{\sqrt{N}} \sum_{\vec{p}} e^{-i\vec{p}\cdot\vec{r}} b_{\alpha\vec{p}}$ (N is a total number of unitcells), the total Hamiltonian (H) in Eqs. (A.1)-(A.3) can be written in a matrix form such as $H = \sum_{\vec{p}} \Psi^\dagger_{\vec{p}} \mathcal{H}_{\vec{p}} \Psi_{\vec{p}}$ for a field of $\Psi_{\vec{p}} = (b_{1\vec{p}}, a_{2\vec{p}}, a_{1\vec{p}}, b_{2\vec{p}})^T$ where

$$\mathcal{H}_{\vec{p}} = \begin{pmatrix} 0 & \xi^*_3(\vec{p}) & \xi_0(\vec{p}) & \xi_4(\vec{p}) \\ \xi_3(\vec{p}) & 0 & \xi^*_4(\vec{p}) & \xi^*_0(\vec{p}) \\ \xi^*_0(\vec{p}) & \xi_4(\vec{p}) & 0 & -\gamma_1 \\ \xi^*_4(\vec{p}) & \xi_0(\vec{p}) & -\gamma_1 & 0 \end{pmatrix}, \quad (A.4)$$

and $\xi_\alpha(\vec{p}) = -\gamma_\alpha \sum_j e^{i\vec{p}\cdot\vec{\delta}_j}$ ($\alpha = 0, 3, 4,\ j = 1, 2, 3$). When we expand Eq. (A.4) around K-point by using $\vec{p} = \vec{k} + \vec{K}$ ($|\vec{k}| \ll |\vec{K}|$) and $\vec{K} = (\frac{4\pi}{3\sqrt{3}} \frac{1}{a_c}, 0)$,

$$\xi_\alpha(\vec{k}+\vec{K}) \simeq -\gamma_\alpha \sum_j e^{i\vec{K}\cdot\vec{\delta}_j} - i\gamma_\alpha \sum_j \vec{k}\cdot\vec{\delta}_j e^{i\vec{K}\cdot\vec{\delta}_j} = v_\alpha(k_x + ik_y), \quad (A.5)$$

where $v_\alpha = \frac{3}{2\hbar}\gamma_\alpha a_c$ ($\alpha = 0, 3, 4$), $\hbar$ is the Planck constant and $\hbar\vec{k} = \hbar(k_x, k_y)$ is the crystal momentum from K-point. The total Hamiltonian near K-point for a field $\Psi_{\vec{k}} = (b_{1\vec{k}}, a_{2\vec{k}}, a_{1\vec{k}}, b_{2\vec{k}})^T$ can be written as

$$\mathcal{H}_{\vec{k}} = \hbar \begin{pmatrix} 0 & v_3 k_- & v_0 k_+ & v_4 k_+ \\ v_3 k_+ & 0 & v_4 k_- & v_0 k_- \\ v_0 k_- & v_4 k_+ & 0 & -\gamma_1 \\ v_4 k_- & v_0 k_+ & -\gamma_1 & 0 \end{pmatrix}, \quad (A.6)$$

where $k_\pm = k_x \pm ik_y$. The effective Hamiltonian ($H_{\text{eff}} + H'_{\text{eff}}$) on the low energy electronic structures for a field $\Psi'_{\vec{k}} = (b_{1\vec{k}}, a_{2\vec{k}})^T$, are described by

$$\mathcal{H}_{\text{eff}} \simeq \hbar v_3 \begin{pmatrix} 0 & k_- \\ k_+ & 0 \end{pmatrix} + \frac{\hbar^2 v_0^2}{\gamma_1} \begin{pmatrix} 0 & k_+^2 \\ k_-^2 & 0 \end{pmatrix}, \quad (A.7)$$

$$\mathcal{H}'_{\text{eff}} \simeq \frac{2\hbar^2 v_0 v_4}{\gamma_1} \begin{pmatrix} k_+k_- & 0 \\ 0 & k_+k_- \end{pmatrix} + \frac{\hbar^2 v_4^2}{\gamma_1} \begin{pmatrix} 0 & k_+^2 \\ k_-^2 & 0 \end{pmatrix}. \quad (A.8)$$

Here we decompose the effective Hamiltonian into $\mathcal{H}_{\text{eff}}$ and $\mathcal{H}'_{\text{eff}}$ where the latter is quite small compared to the former. By using Pauli spin matrices, $\tau_0 = \left(\begin{smallmatrix} 1 & 0 \\ 0 & 1 \end{smallmatrix}\right)$, $\tau_x = \left(\begin{smallmatrix} 0 & 1 \\ 1 & 0 \end{smallmatrix}\right)$, and $\tau_y = \left(\begin{smallmatrix} 0 & -i \\ i & 0 \end{smallmatrix}\right)$, the above Eqs. (A.7) and (A.8) can be written in compact forms,

$$\mathcal{H}_{\text{eff}} \simeq \hbar v_3 \vec{\tau}\cdot\vec{k} + \frac{\hbar^2 v_0^2}{\gamma_1} (\vec{\tau}^*\cdot\vec{k}) \tau_x (\vec{\tau}^*\cdot\vec{k}), \quad (A.9)$$

$$\mathcal{H}'_{\text{eff}} \simeq \frac{2\hbar^2 v_0 v_4}{\gamma_1} |\vec{k}|^2 \tau_0 + \frac{\hbar^2 v_4^2}{\gamma_1} (\vec{\tau}^*\cdot\vec{k}) \tau_x (\vec{\tau}^*\cdot\vec{k}), \quad (A.10)$$

where $\vec{\tau} = (\tau_x, \tau_y)$ and $\vec{\tau}^*$ is its complex conjugate. Hereafter, we will neglect the smallest hopping parameter γ_4 (Eqs. (A.8) and (A.10)) and discuss its role later.

The effective Hamiltonian in Eq. (A.9) gives energy eigenvalues

$$E(\vec{k}) = \pm\hbar v_3 k \left| 1 + \frac{k}{p_D} e^{3i\phi_k} \right|, \quad (A.11)$$

where $k = |\vec{k}|$, $\phi_k = \tan^{-1}(k_y/k_x)$ and $p_D = \gamma_1 v_3/(\hbar v_0^2) = 2/(3a_c)\gamma_1\gamma_3/\gamma_0^2$.

When the layer 2 (bottom layer) slides against the layer 1 (top) along $\vec{d}_s = (d_x, d_y)$ ($|\vec{d}_s| \ll a_c$) [Figs. 1(a) and (b)], the constant nnn inter-layer interaction (γ_3) now depends on the carbon pair distance in layer 1 and 2 [Fig. 1(d)] and nn inter-layer interaction (γ_1) decreases to γ'_1. Since we focus on an extremely small sliding distance, we assume variation of the nnn inter-layer interaction such as $\gamma_3 \to \gamma_3(\vec{\delta}_i) \simeq \gamma_3 e^{-\beta\vec{\delta}_i\cdot\vec{d}_s} \simeq \gamma_3(1 - \beta\vec{\delta}_i\cdot\vec{d}_s)$ where $i = 1, 2, 3$ and β is a positive real constant. When we expand Eq. (A.4) around K-point including sliding effect, intra-layer interactions remain the same as before. However, unlike the expansion procedure without sliding shown in Eq. (A.5), the interlayer interaction with sliding can be

expanded up to a leading order of $\vec{k}$ and $\vec{d}$ as

$$\begin{aligned}\xi_3(\vec{k}+\vec{K}) &\simeq -\sum_j \gamma_3(\vec{\delta}_j)e^{i(\vec{k}+\vec{K})\cdot\vec{\delta}_j} \\ &\simeq -\sum_j \gamma_3(1-\beta\vec{\delta}_i\cdot\vec{d}_s)(1+i\vec{k}\cdot\vec{\delta}_j)e^{i\vec{K}\cdot\vec{\delta}_j} \\ &\simeq \hbar v_3(k_x+ik_y)+\hbar v_3\beta(id_x-d_y). \quad \text{(A.12)}\end{aligned}$$

Hence, the sliding vector d_s plays a role of shifting the nnn intra-layer Hamiltonian in momentum space like a constant vector potential. With γ_4 neglected, the total Hamiltonian near K-point in Eq. (A.6) now transforms to

$$\mathcal{H}_{\vec{k}} = \hbar\begin{pmatrix} 0 & v_3(k_- - \lambda_-) & v_0k_+ & 0 \\ v_3(k_+ - \lambda_+) & 0 & 0 & v_0k_- \\ v_0k_- & 0 & 0 & -\gamma_1' \\ 0 & v_0k_+ & -\gamma_1' & 0 \end{pmatrix} \quad \text{(A.13)}$$

where $\lambda_\pm = \beta(d_y \mp id_x)$. Here we neglect an overall phase shift of $e^{i\vec{d}_s\cdot\vec{k}}$ because of $|\vec{d}_s| \ll a_c$. The effective low energy Hamiltonian of Eq. (A.9) also changes to

$$\mathcal{H}_{\text{eff}} \simeq \hbar v_3\vec{\tau}\cdot(\vec{k}-\vec{\lambda}) + \frac{\hbar^2 v_0^2}{\gamma_1'}(\vec{\tau}^*\cdot\vec{k})\tau_x(\vec{\tau}^*\cdot\vec{k}) \quad \text{(A.14)}$$

where $\vec{\lambda} \equiv (\lambda_x, \lambda_y) = \beta(d_y, -d_x) = \beta(\vec{d}_s \times \hat{k}_z)$ ($\hat{k}_z = \hat{k}_x \times \hat{k}_y$ and $(\hat{k}_x, \hat{k}_y) = \vec{k}/|\vec{k}|$).

Now, let us consider the smallest interlayer interaction γ_4 with sliding. When sliding occurs, γ_4 shown in Fig. 1(e) becomes anisotropic and depends on the pair distances between relevant carbon atoms in the top and bottom layer. We find that $\gamma_4 \to \gamma_4(\vec{\delta}_i) \simeq \gamma_4 e^{\beta\vec{\delta}_i\cdot\vec{d}_s} \simeq \gamma_4(1+\beta\vec{\delta}_i\cdot\vec{d}_s)$ where $i = 1, 2, 3$. Here we assume the same coefficient β of $\gamma_3(\vec{\delta}_i)$ for calculation convenience and note that it does not change the main conclusions of the paper. Like Eq. (A.12) for γ_3, we can expand ξ_4 as

$$\begin{aligned}\xi_4(\vec{k}+\vec{K}) &\simeq -\sum_j \gamma_4(\vec{\delta}_j)e^{i(\vec{k}+\vec{K})\cdot\vec{\delta}_j} \\ &\simeq -\sum_j \gamma_4(1+\beta\vec{\delta}_i\cdot\vec{d}_s)(1+i\vec{k}\cdot\vec{\delta}_j)e^{i\vec{K}\cdot\vec{\delta}_j} \\ &\simeq \hbar v_4(k_x+ik_y)-\hbar v_4\beta(id_x-d_y) \\ &= \hbar v_4 k_+ + \hbar v_4\lambda_+. \quad \text{(A.15)}\end{aligned}$$

With γ_4 included, now the total Hamiltonian near K-point in Eq. (A.13) has an additional term,

$$\mathcal{H}_{\vec{k}} = \hbar v_4\begin{pmatrix} 0 & 0 & 0 & k_+ + \lambda_+ \\ 0 & 0 & k_- + \lambda_- & 0 \\ 0 & k_+ + \lambda_+ & 0 & 0 \\ k_- + \lambda_- & 0 & 0 & 0 \end{pmatrix} \quad \text{(A.16)}$$

Then, Eq. (A.10) changes to

$$\begin{aligned}\mathcal{H}'_{\text{eff}} &\simeq \frac{2\hbar^2 v_0 v_4}{\gamma_1}\vec{k}\cdot(\vec{k}+\vec{\lambda})\tau_0 \\ &+ \frac{\hbar^2 v_4^2}{\gamma_1}[\vec{\tau}^*\cdot(\vec{k}+\vec{\lambda})]\tau_x[\vec{\tau}^*\cdot(\vec{k}+\vec{\lambda})]. \quad \text{(A.17)}\end{aligned}$$

* Electronic address: hand@kias.re.kr
† Electronic address: jhish@postech.ac.kr

[1] I. M. Lifshitz, Sov. Phys. JETP **21**, 1130 (1960).
[2] Y. M. Blanter, M. I. Kaganov, A. V. Pantsulaya, and A. A. Varlamov, Phys. Rep **245**, 159 (1994).
[3] A. A. Varlamov, V. S. Egorov, and A. V. Pantsulaya, Adv. Phys **38**, 469 (1989).
[4] N. P. Armitage, R. Tediosi, F. Lévy, E. Giannini, L. Forro, and D. van der Marel, Phys. Rev. Lett. **104**, 237401 (2010).
[5] K. S. Novoselov, E. McCann, S. V. Morozov, V. I. Fal'ko, M. I. Katsnelson, U. Zeitler, D. Jiang, F. Shedin, and A. K. Geim, Nat. Phys. **2**, 177 (2006).
[6] G. Li, A. Luican, J. M. B. Lopes dos Santos, A. H. Castro Neto, A. Reina, J. Kong, and E. Y. Andrei, Nat. Phys. **6**, 109 (2009).
[7] B. E. Feldman, J. Martin, and A. Yacoby, Nat. Phys. **5**, 889 (2009).
[8] R. T. Weitz, M. T. Allen, B. E. Feldman, J. Martin, and A. Yacoby, Science **330**, 812 (2010).
[9] Y. Lemonik, I. L. Aleiner, C. Toke, and V. I. Fal'ko, Phys. Rev. B **82**, 201408 (2010).
[10] E. McCann and V. I. Fal'ko, Phys. Rev. Lett. **96**, 086805 (2006).
[11] M. Koshino and T. Ando, Phys. Rev. B **73**, 245403 (2006).
[12] J. Nilsson, A. H. Castro Neto, F. Guinea, and N. M. R. Peres, Phys. Rev. B **78**, 045405 (2008).
[13] J. Cserti, A. Csordás, and G. Dávid, Phys. Rev. Lett. **99**, 066802 (2007).
[14] H. Min, B. Sahu, S. K. Banerjee, and A. H. MacDonald, Phys. Rev. B **75**, 155115 (2007).
[15] A. H. Castro Neto, F. Guinea, N. M. R. Peres, K. S. Novoselov, and A. K. Geim, Rev. Mod. Phys. **81**, 109 (2009).
[16] E. V. Castro, N. M. R. Peres, T. Stauber, and N. A. P. Silva, Phys. Rev. Lett. **100**, 186803 (2008).
[17] R. Nandkishore and L. Levitov, Phys. Rev. Lett. **104**, 156803 (2010).
[18] F. Zhang, H. Min, M. Polini, and A. H. MacDonald, Phys. Rev. B **81**, 041402 (2010).
[19] O. Vafek and K. Yang, Phys. Rev. B **81**, 041401 (2010).
[20] J. M. B. Lopes dos Santos, N. M. R. Peres, and A. H. Castro Neto, Phys. Rev. Lett. **99**, 256802 (2007).
[21] S. Shallscross, S. Sharma, and O. A. Pankratov, Phys. Rev. Lett. **101**, 056803 (2008).
[22] J. Hass, F. Varchon, J. E. Mill'a-Otoya, M. Sprinkle, N. Sharma, W. A. de Heer, C. Berger, P. N. First, L. Magaud, and E. H. Conrad, Phys. Rev. Lett. **100**, 125504 (2008).
[23] P. Giannozzi, S. Baroni, N. Bonini, M. Calandra, R. Car, C. Cavazzoni, D. Ceresoli, G. L. Chiarotti, M. Cococ-

cioni, I. Dabo, A. Dal Corso, S. de Cironcoli, S. Fabris, G. Fratesi, R. Gebauer, U. Gerstman, C. Gougoussis, A.Kokalj, M. Lazzeri, L. Martin-Samos, N. Marzari, F. Mauri, R. Mazzarello, S. Paolini, A. Pasquarello, L. Paulatto, C. Sbraccia, S. Scandolo, G. Sclauzero, A. P. Seitsonen, A. Smogunov, P. Umari,and R. M. Wentzcovitch, J. Phys.:Condens. Matter **21**, 395502 (2009).

[24] J. P. Perdew, K. Burke, and M. Ernzerhof, Phys. Rev. Lett. **77**, 3865 (1996).

[25] D. Vanderbilt, Phys. Rev. B **41**, 7892 (1990).

[26] N. Marzari, D. Vanderbilt, A. De Vita, and M. C. Payne, Phys. Rev. Lett. **82**, 3296 (1999).

[27] G. Kresse and J. Hafner, Phys. Rev. B **49**, 14251 (1994).

[28] S. Grimme, J. Comput. Chem. **27**, 1787 (2006).

[29] V. Barone, M. Casarin, D. Forrer, M. Pavone, M. Sambi, and A. Vittadini, J. Comput. Chem. **30**, 934 (2008).

[30] A. N. Kolmogorov and V. H. Crespi, Phys. Rev. Lett. **85**, 4727 (2000).

[31] Q. Wu and W. Yang, J. Chem. Phys. **116**, 515 (2002).

[32] T. Gould, K. Simpkins, and J. F. Dobson, Phys. Rev. B **77**, 165134 (2008).

[33] L. Spanu, S. Sorella, and G. Galli, Phys. Rev. Lett. **103**, 196401 (2009).

[34] S. Grimme, G. Mück-Lichtenfeld, and J. Antony, J. Phys. Chem. C **111**, 11199 (2007).

[35] S. D. Chakarova-Käck, E. Schröder, B. I. Lundqvist, and D. C. Langreth, Phys. Rev. Lett. **96**, 146107 (2006).

[36] A. B. Kuzmenko, I. Crassee, D. van der Marel, P. Blake, and K. S. Novoselov, Phys. Rev. B **80**, 165406 (2009).

[37] V. M. Pereira, A. H. Castro Neto, and N. M. R. Peres, Phys. Rev. B **80**, 045401 (2009).

[38] S.-M. Choi, S.-H. Jhi, and Y.-W. Son, Phys. Rev. B **81**, 081407 (2010).

[39] F. Guinea, M. I. Katsnelson, and A. K. Geim, Nat. Phys. **6**, 30 (2010).

[40] S.-M. Choi, S.-H. Jhi, and Y.-W. Son, Nano Lett. **10**, 3486 (2010).

[41] Y. J. Song, A. F. Otte, Y. Kuk, Y. Hu, D. B. Torrance, P. N. First, W. A. de Heer, H. Min, S. Adam, M. D. Stiles, A. H. MacDonald and J. A. Stroscio, Nature **467**, 185 (2010).

[42] G. Montambaux, F. Piéchon, J.-N. Fuchs, and M. O. Goerbig, Phys. Rev. B **80**, 153412 (2009).

[43] B. Wunsch, F. Guinea, and F. Sols, New. J. Phys. **10**, 103027 (2008).

[44] G. P. Mikitik and Y. V. Sharlai, Phys. Rev. Lett. **82**, 2147 (1999).

[45] P. Dietal, F. Piéchon, and G. Montambaux, Phys. Rev. Lett. **100**, 236405 (2008).

[46] A. Bermudez, N. Goldman, A. Kubasiak, M. Lewenstein, and M. A. Martin-Delgado, New. J. Phys. **12**, 033041 (2010).

[47] Y. Hosotani, Phys. Lett. **129B**, 193 (1983).

[48] M. Mucha-Kruczynski, I. L. Aleiner, and V. I. Fal'ko, Phys. Rev. B **84**, 041404 (2011).

[49] R. de Gail, M. O. Goerbig, F. Guinea, G. Montambaux, and A. H. Castro Neto, Phys. Rev. B **84**, 045436 (2011).

[50] A. S. Mayorov, D. C. Elias, M. Mucha-Kruczynski, R. V. Gorbachev, T. Tudorovskiy, A. Zhukov, S. V. Morozov, M. I. Katsnelson, V. I. Fal'ko, A. K. Geim, and K. S. Novoselov, Science **333**, 860 (2011).